RSC Advances

PAPER

View Article Online
View Journal | View Issue

Cite this: *RSC Adv.*, 2017, **7**, 36902

A facile approach for photoelectrochemical performance enhancement of CdS QD-sensitized TiO_2 *via* decorating {001} facet-exposed nano-polyhedrons onto nanotubes†

Dong Ding, Bo Zhou, Shurong Liu, Guijie Zhu, Xianwei Meng, Jiandong Yang, Wuyou Fu and Haibin Yang*

In this study, we report a TiO_2 hybrid structure prepared by a facile route, wherein TiF_6^{2-} ion has been used as both the surfactant and titanium source. Single-crystalline TiO_2 nano-polyhedrons with exposed high active {001} facets were grown on a TiO_2 nanowire and nanotube (TWTs) films. This hybrid structure served as a model architecture for efficient photoelectrochemical (PEC) devices because it simultaneously offered a large contact area with the electrolyte and direct pathway for photoexcited electron collection. Under simulated sunlight illumination (AM 1.5 light at 100 mW cm^{-2}), this hybrid structure exhibited a photocurrent density of 1.36 mA cm^{-2} at 0 V *vs.* Ag/AgCl (J_{SC}) and photoconversion efficiency (η) of 0.81% at −0.51 V *vs.* Ag/AgCl, nearly 2.4 times higher than those of the bare TWTs. Morphology of the TiO_2 nano-polyhedrons in the hybrid structure was greatly influenced by the TiF_6^{2-} ion concentration, and a proper concentration was determined to be 2.5 mM. Moreover, the CdS QDs were sensitized onto the hybrid structure, and their J_{SC} and η reached 2.31 mA cm^{-2} & 1.94%, respectively, 1.5 times higher than those of the CdS-sensitized bare TWTs. The TiO_2 nano-polyhedrons improved the efficiency *via* increasing the specific surface area of the electrode, thus facilitating hole transfer into the electrolyte. Moreover, the exposed high reactive {001} facets provided more effective area for the adsorption of CdS, leading to an enhanced photogeneration carrier density.

Received 23rd May 2017
Accepted 13th July 2017

DOI: 10.1039/c7ra05772e

rsc.li/rsc-advances

1. Introduction

Anatase TiO_2 has been vastly explored in solar energy conversion owing to its advantages of favorable photooxidation power, easy availability, good chemical stability, and nontoxicity,[1,2] which has outstanding performances as photoelectrodes in photoelectrochemical (PEC) fields such as in photocatalysis, photovoltaics, and water splitting.[3–7] PEC performance is mainly determined by the amount of photo-generated electron–hole pairs, which are driven by large specific surface area and high photoactivity of the TiO_2 photoanode according to the Honda–Fujishima effect.[8–10] The TiO_2 hybrid structure, which can combine the advantages of different morphologies and effectively enlarge specific surface area, is an ongoing hot research topic.[11–16] Y. Tang *et al.* have grown TiO_2 nanoparticles on TiO_2 nanoflakes; the obtained hierarchical porous hybrid structure has a larger specific surface area than the TiO_2 nanosheets and nanoparticles and higher photocatalytic activity for the degradation of organic compounds.[17] Dongsheng Xu *et al.* have prepared hetero-structured TiO_2 nanotree arrays with rutile trunks and anatase branches. The hybrid structure can deposit more CdS/CdSe QDs and improve the conversion efficiency of the whole device.[18] Compared with TiO_2 nanostructures in other forms, highly ordered TiO_2 nanotubes and nanowires (TWTs) are anticipated to possess unidirectional electrical channels and high specific surface area, which show promising properties due to their slower recombination and higher charge collection efficiency. Therefore, a structural modification strategy for preparing a hybrid structure based on TWTs is highly desirable.

Moreover, PEC performance of TiO_2 is closely associated with its exposed facets; theoretical and experimental studies reveal that the {001} facets achieve higher chemical activities than {101} and {100} facets in the anatase TiO_2 crystals (the average surface energies of anatase TiO_2 are in the order γ {001} (0.90 J m^{-2}) > γ {100} (0.53 J m^{-2}) > γ {101} (0.44 J m^{-2})).[19] This can be attributed to the larger Ti–O–Ti bond angle on the {001}

State Key Laboratory of Superhard Materials, Jilin University, Changchun 130012, P. R. China. E-mail: yanghb@jlu.edu.cn; Tel: +86 431 85168763

† Electronic supplementary information (ESI) available: Fig. S1 TEM images of hybrid structure. Fig. S2 XPS spectrum of hybrid structure. Fig. S3 PEC performance of hybrid structure samples prepared under different TiF_6^{2-} concentration: *J–V* curves (A), photoconversion efficiencies (B). Fig. S4 SEM images of bare TWTs (A and B), CdS sensitized bare TWTs (C and D). Fig. S5 line scan profile of EDX spectra of CdS sensitized hybrid structure. See DOI: 10.1039/c7ra05772e

facets, which make the 2p states of the surface O atoms unstable and very reactive.[20] However, according to the Wulff construction, the {001} facets tend to diminish during the free crystal growth process to minimize the total surface energy.[21,22] Surfactant-assisted method is a popular approach for the controlled synthesis of {001} facet-exposed anatase TiO_2, in which F^- are introduced as surfactants.[23,24] Lu *et al.* used TiF_4 and HF as raw materials in a Teflon-lined autoclave to prepare {001} facet-exposed TiO_2 single crystals and found that the {001} facets played crucial roles in photoreactivity improvement of TiO_2.[25,26] Pan *et al.* have prepared N + Ni co-doped anatase TiO_2 nanocrystals with exposed {001} facets using a two-step hydrothermal reaction, and the as-prepared sample showed a superior photocatalytic activity.[27] The synthesized TiO_2 single crystals and TWT hybrid structure with highly reactive {001} facets can have potential applications in several areas such as in photocatalytic CO_2 reduction, solar cells, and photonic and optoelectronic devices.

In this study, we synthesized a novel TiO_2 hybrid structure *via* a facile route, as illustrated in Scheme 1. First, highly ordered TiO_2 nanotubes and nanowires (TWTs) on a Ti foil were prepared by electrochemical anodization. Second, single-crystalline TiO_2 nano-polyhedrons with exposed {001} facets were grown on TWTs through a chemical bath deposition (CBD) process under atmospheric pressure, wherein TiF_6^{2-} was used as both the surfactant and titanium source. We conducted varied TiF_6^{2-} concentration studies during the CBD process and proposed a possible growth mechanism. Third, CdS QDs were assembled onto bare TWTs and hybrid structure *via* successive ionic layer adsorption and reaction (SILAR) technique. CdS ($E_g \approx 2.4$ eV) sensitization is considered as an effective method to broaden the solar absorption spectrum of TiO_2 ($E_g \approx 3.2$ eV). Thus, we obtained a hybrid structure with superior PEC performance than bare TWTs owing to its preponderances of increased surface area and exposed highly reactive {001} facets.

2. Experimental

2.1 Preparation of the hybrid structure

Bare TWTs were prepared *via* electrochemical anodization of a Ti foil (99.9% purity) using a direct current (dc) stabilized voltage and current power supply (WYJ60V3A, Pingguo Instrumentation Co. Ltd. China) at a constant voltage of 40 V for 1 h. The Ti foil and a graphite plate were used as the anode and cathode, respectively. Electrolyte solution contained 0.3 wt% NH_4F, 95.0 vol% ethylene glycol, and 5.0 vol% deionized H_2O. The as-prepared photoelectrode was thoroughly washed with ethanol and DI water and then annealed in air at 450 °C for 2 h. TiO_2 nano-polyhedrons were grown on TWTs *via* chemical bath deposition, *i.e.*, TWTs were immersed in an aqueous solution containing 2.5 mM $(NH_4)_2TiF_6$ at 80 °C for 30 min; then, the sample was washed with DI water and annealed in air at 450 °C for 1 h.

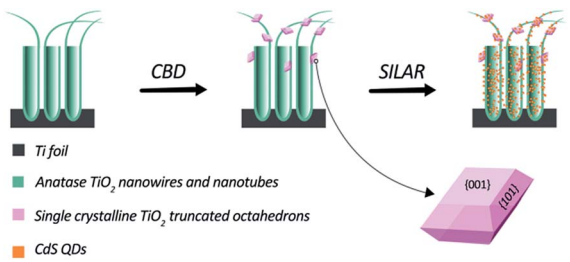

Scheme 1 Schematic of the preparation process.

2.2 Preparation of the CdS-sensitized hybrid structure

In detail, the sample was successively immersed in 0.5 M mercaptoacetic acid (TGA) and then in 0.5 M $Cd(NO_3)_2 \cdot 4H_2O$ in ethanol and finally in 0.5 M Na_2S in deionized water. Each immersion was performed for 10 min; the photoelectrode was then rinsed successively with pure ethanol and deionized water to remove excess precursors and dried in air before the next dipping cycle. This abovementioned process was repeated six times. CdS-sensitized bare TWTs were prepared under the same conditions for comparison.

2.3 Sample characterization

Scanning electron microscopy (SEM) images were obtained using a field-emission SEM (JEOL JSM-6700F). Transmission electron microscopy (TEM) and high-resolution TEM (HRTEM) images and EDS mapping were obtained using a JEM-2100F high-resolution transmission microscope operating at 200 kV. Optical characterization (UV-vis absorption spectra) of the film was performed using a UV-3150 double-beam spectro-photometer (Shimadzu UV-3150). X-ray diffraction (XRD) spectra of the samples were obtained using a Rigaku D/max-2500 X-ray diffractometer with Cu Kα radiation ($\lambda = 1.5418$ Å).

PEC performance of the samples was analysed *via* an electrochemical workstation (CH Instruments, model CHI601C) using a Ag/AgCl reference electrode and a Pt wire as the counter electrode. A 500 W Xe lamp (Spectra Physics) with a monochromator simulated sunlight, which was adjusted to provide AM 1.5 light at 100 mW cm^{-2} using a laser power meter (BG26M92C, Midwest Group). The electrolyte solution consisted of 0.25 M $Na_2S \cdot 9H_2O$, 0.35 M Na_2SO_3, and 0.1 M KCl aqueous solution (pH = 12). The photoconversion efficiency (η) was calculated from the line sweep voltammogram as follows:[28,29]

$$\eta = J_{SC}(E^o - E)/I$$

where J_{SC} is the photocurrent density (mA cm^{-2}); I is the power density of incident light (mW cm^{-2}); E^o is 1.23 V/NHE; and E is the applied potential *vs.* RHE, which is given by the Nernst equation $E = E_{Ag/AgCl} + 0.059$ pH + 0.197 V.

The IPCE of the samples were measured using a two-electrode system with an action spectrum measurement setup (PEC-S20, Peccell Ltd.). Before the measurement, the samples were sealed in sandwich structures with a 60 μm spacer using Pt as the counter electrode. The electrolyte was injected between the two electrodes. Light was irradiated from the counter electrode side.

3. Results and discussion

For obtaining TiO_2 hybrid structures, 2.5 mM TiF_6^{2-} bath was taken out for 30 minutes as an additional treatment after the traditional anodizing process. Fig. 1A and B show the top-view and side-view SEM images of the as-prepared sample, respectively. Herein, three major morphologies, *i.e.* nanotubes, nanowires, and nano-polyhedrons, can be observed. Nanotubes with a split top are highly orderly arranged and exhibit an average length of ~3 μm and diameter of ~73.3 nm (Fig. S1 in ESI†). Nano-polyhedrons (truncated octahedrons) are grown on both side and split top sites of the TWTs with an average size of ~91.5 nm, and the relative TEM images are shown in the ESI (Fig. S2†). Fig. 1C shows the HRTEM and fast Fourier transform (FFT) images of the selected area of nano-polyhedrons. Interplanar spacings of 0.352 nm and 0.475 nm with an interfacial angle of 68.3° are consistent with those of the (101) and (002) facets of anatase TiO_2 (JCPDS no. 71-1167), respectively. FFT patterns in the inset refer to the (101) and (002) facets. Furthermore, a (101) zone-axis could be deduced, where the exposed surfaces were bound by the {101} and {001} facets. Fig. 1D shows the interface of the nanowire and nano-polyhedron. A clear boundary further confirms that single-crystalline nano-polyhedrons are bonded on nanowires. The crystal structure of the hybrid structure is examined by X-ray diffraction (XRD), as shown in Fig. 1E. The diffraction peaks are indexed to the anatase-phase TiO_2 (JCPDS no. 71-1167) and Ti, further demonstrating that the as-synthesized hybrid structure grown on Ti is pure anatase TiO_2.

In a typical anodizing system, Ti is corroded into TiF_6^{2-} by F^- under electric current; thereafter, TiF_6^{2-} hydrolyses into $Ti(OH)_4$, and the stacking blocks of the nanotube. Then, the nanotubes undergo an annealing process in which Ti–O–Ti are joined *via* dehydration. When the sample is merged into the TiF_6^{2-} solution, TiO_2 nucleates on nanotubes and grows into nano-polyhedrons. Fig. 2 and S3† show the SEM images of the samples synthesized at the TiF_6^{2-} concentration of 0.5 mM, 1.5 mM, 2.5 mM, and 3.5 mM (denoted as S-0.5/1.5/2.5/3.5, respectively). As TiF_6^{2-} concentration increases from 0.5 mM to 2.5 mM, the grain size of the polyhedron increases from 22.5 nm to 91.5 nm and the shape becomes regular. We deduced that the TiO_2 nano-polyhedrons were formed through the hydrolysis of TiF_6^{2-} through the following reaction:

$$[TiF_6]^{2-} + nH_2O \leftrightarrow [Ti(OH)_nF_{6-n}]^{2-} + nHF$$

$$[Ti(OH)_6]^{2-} + 2H^+ \rightarrow TiO_2 + 4H_2O$$

Usually, TiO_6^{2-} octahedra are the building blocks of TiO_2. As illustrated in Fig. 2E, F^- generated by hydrolysis process could favorably adsorb on the high active {001} facets of TiO_2 and suppress the growth along the [001] direction. Consequently,

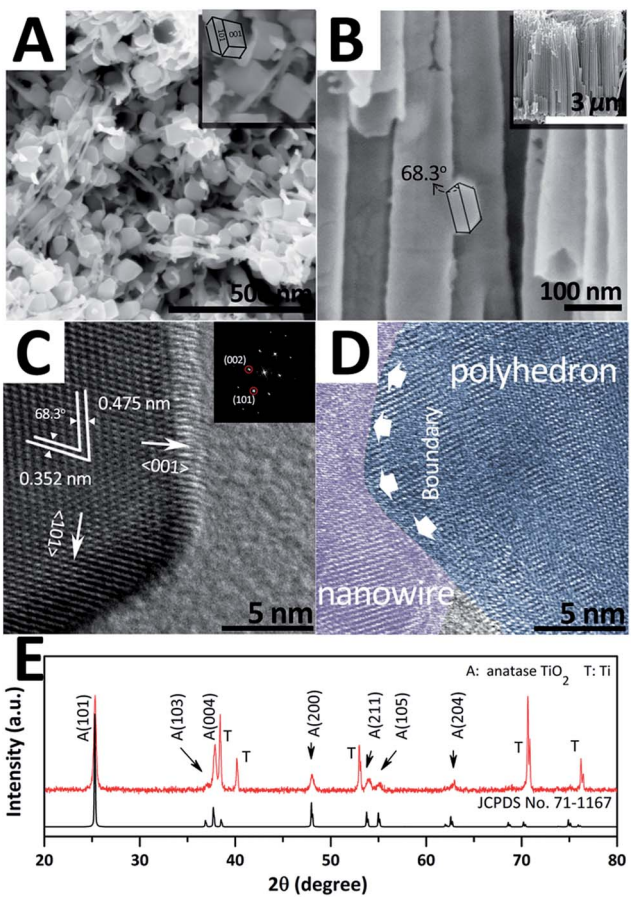

Fig. 1 SEM images (A and B), HRTEM and FFT images (C and D), and XRD pattern (E) of hybrid structure.

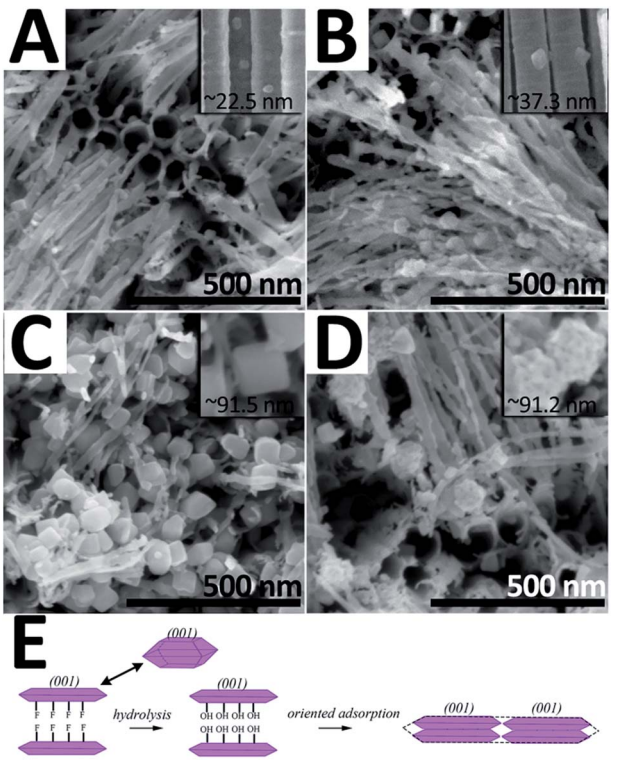

Fig. 2 SEM images of the hybrid structure synthesized at varied TiF_6^{2-} concentrations: 0.5 mM (A), 1.5 mM (B), 2.5 mM (C), and 3.5 mM (D). Schematic showing the TiO_2 nano-polyhedron formation (E).

the resulting TiO_2 crystal nucleus maintains the {001} facet-exposed truncated octahedral structure.[25] When the TWTs are immersed in TiF_6^{2-} solution, TiO_2 nucleates on TWTs and grows into nano-polyhedrons. When the TiF_6^{2-} concentration increases, the surface of these {001} facets-exposed TiO_2 crystal nucleus hydrolyzes and F^- would be replaced by hydroxyl groups; then, the oriented adsorption process occurs under the influence of dehydration condensation reaction between hydroxyl groups. Hence, the size of the TiO_2 nano-polyhedrons becomes larger. This indicates that at this stage, the TiF_6^{2-} concentration is the main parameter affecting the growth of the polyhedrons; as the TiF_6^{2-} concentration increases, the system can afford enough growth dynamic to gradually form an entire (001) low-energy surface. However, when the TiF_6^{2-} concentration further increases to 3.5 mM, the grain size remains ~91 nm, but the surfaces become rough. This can be attributed to further nucleation on the polyhedron surfaces caused by extreme undercooling.

PEC performance of the hybrid structure samples prepared at different TiF_6^{2-} concentrations is shown in Fig. S6.† The S-2.5 sample shows the best PEC performance owing to the greater specific surface area and exposed {001} facets. On the other hand, when the TiF_6^{2-} concentration reaches 3.5 mM, randomly deposited TiO_2 crystal nuclei on the nano-polyhedrons cover the high active {001} facets and result in a decreased J_{SC} and η. In this study, the S-2.5 sample has been chosen for the following CdS QD sensitization investigation. The CdS QD-sensitized bare TWTs were prepared and investigated for comparison.

The as-prepared hybrid structure samples were further sensitized by CdS QDs, as shown in Fig. 3. Fig. 3A and B show the top- and side-view SEM images. The surfaces of the arrayed TWTs and nano-polyhedrons are decorated by evenly distributed CdS QDs and become rough. Moreover, the CdS QDs on the TWTs and nano-polyhedrons are investigated by HRTEM, as shown in Fig. 3C and D, respectively. The average size of the CdS QDs is ~5.3 nm. The *d*-spacings of the clear crystalline structure are 0.335 nm, 0.205 nm, and 0.352 nm, that can be indexed to (111) and (220) of CdS (JCPDS no. 80-0019) and (101) of anatase TiO_2, respectively. EDS mapping of the sample is shown in Fig. 3E and the corresponding line scan profile of EDX spectra is shown in the ESI (Fig. S9†). The distribution and counts of the Cd and S elements are very similar, but different from those of the Ti and O elements; this indicates that the CdS crystal is the only form in which Cd and S exist. Fig. 3F shows the UV-vis spectra of the original sample and the sensitized sample. The absorption range greatly enlarges from ~380 nm to 570 nm. The tuned band gap indicates that CdS QDs are well bonded onto the TiO_2 hybrid structure and provide a good electronic transmission channel. Fig. 3G shows the XRD patterns of the sample. A new peak at $2\theta = 26.5°$ is observed and indexed to CdS, which is in accordance with the abovementioned HRTEM results.

Photocurrent is usually seen as one of the key parameters of PEC performance and reflects the transfer efficiency of photo-excited electrons. Fig. 4A presents the photocurrent density characteristics (*J*–*V* curves) and photoconversion efficiencies of the samples. The photocurrent density at 0 V *vs.* Ag/AgCl (J_{SC})

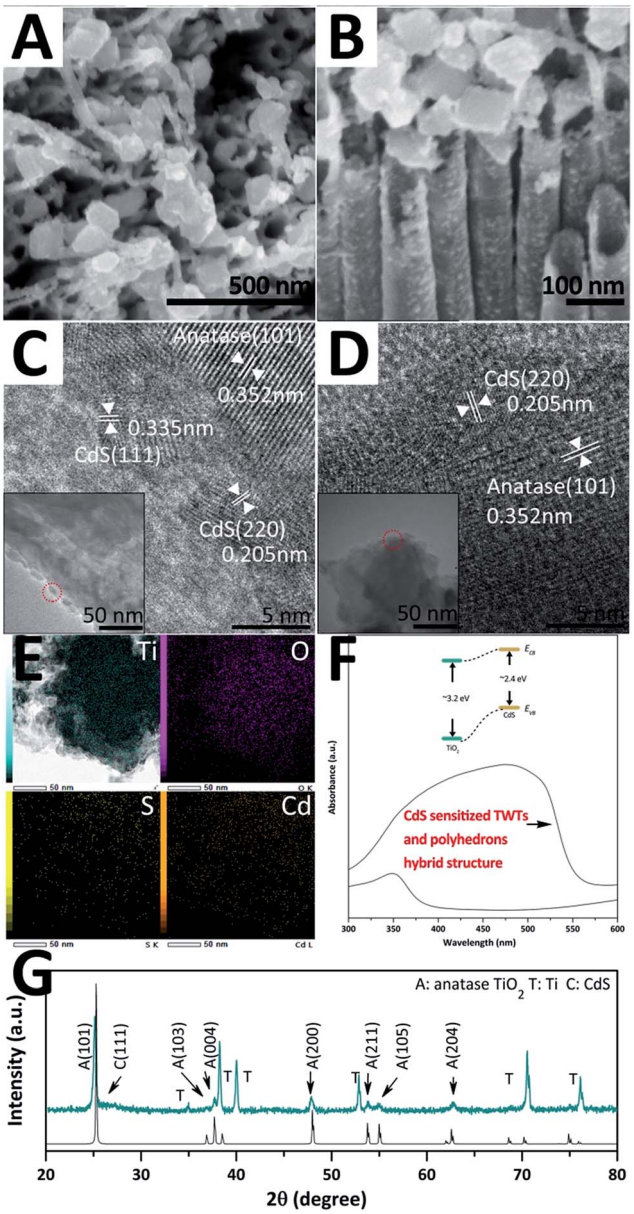

Fig. 3 SEM images (A and B), TEM and HRTEM images (C and D), EDS mapping (E), UV-vis spectra (F), and XRD patterns (G) of the CdS-sensitized hybrid structure.

and photoconversion efficiency (η) of the hybrid structure are 1.36 mA cm^{-2} and 0.81% (−0.51 V *vs.* Ag/AgCl), respectively, nearly 2.4 times higher than those of bare TWTs (0.57 mA cm^{-2} and 0.35% at −0.42 V *vs.* Ag/AgCl). Furthermore, J_{SC} and η of 1.53 mA cm^{-2} and 1.14% (−0.69 V *vs.* Ag/AgCl), respectively, were attained for the CdS-sensitized TWTs. These results confirm that CdS QD sensitization is an effective method for enhancing the PEC performance of TWTs. The J_{SC} and η of the CdS-sensitized hybrid structure are found to be 2.31 mA cm^{-2} and 1.94% (−0.65 V *vs.* Ag/AgCl), respectively, about 1.5 times those of the CdS-sensitized bare TWTs, and the hybrid structure can boost the J_{SC} and η of bare TWTs by up to 400%. Moreover, the PEC performance of the electrodes at various wavelengths was measured by the IPCE test. As shown in Fig. 4B, the best

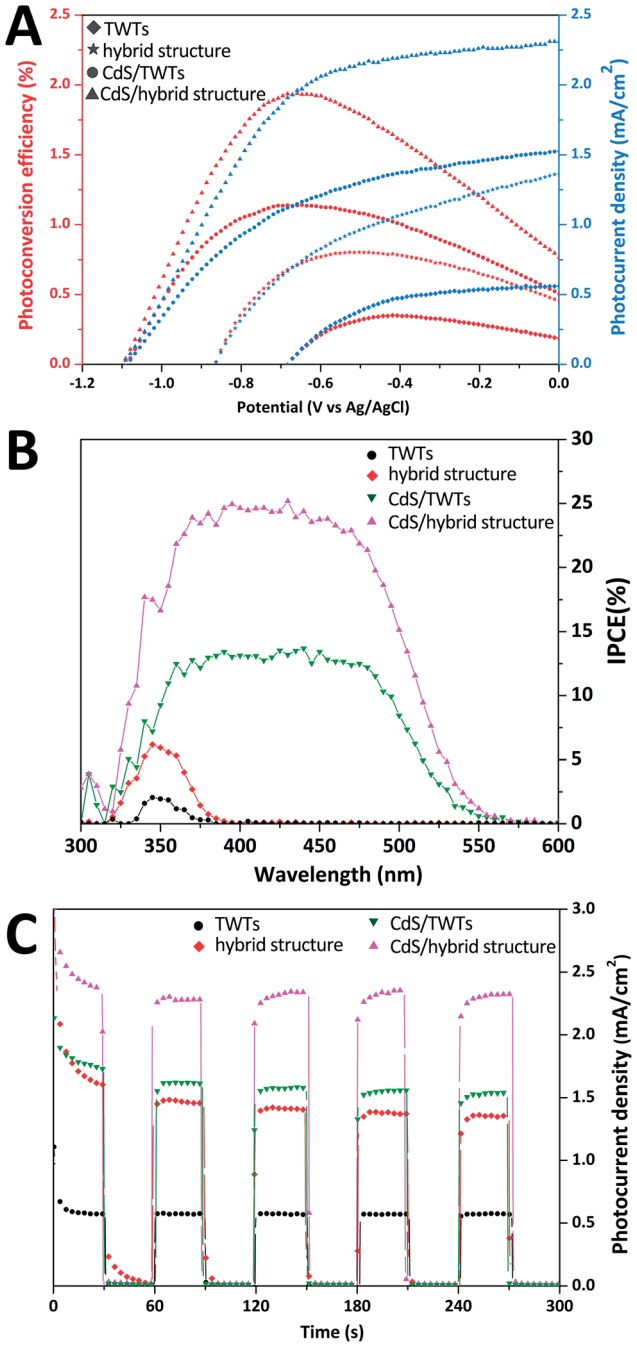

Fig. 4 *J–V* curves and photoconversion efficiencies (A), IPCE data (B), and *J–T* curves under chopped illumination (C) of TWTs, hybrid structure, CdS-sensitized TWTs, and CdS-sensitized hybrid structure.

IPCE of the CdS-sensitized hybrid structure electrode is around 25% across the absorption ranges, which is higher than those of other electrodes (14% for CdS-sensitized TWTs > 6% for hybrid structure > 2% for TWTs), indicating that electron–hole pairs are more efficiently separated in the CdS-sensitized hybrid structure electrode. IPCE results of the samples are in accordance with the corresponding absorption spectra as well as the corresponding photocurrent–voltage (*J–V*) curves. Stability, reproducibility, and repeatability of the samples can be represented by transient photocurrent (*J–T*) plots. We generated the *J–T* plots at 0 V *vs.* Ag/AgCl under chopped illumination. The *J–T* responses of the samples are shown in Fig. 4C; all the samples show relatively good reproducibility and stability when illumination is turned on and off. The observed dark current densities (light off) for all the samples are negligible. It is obvious that the effect of CdS is more prominent in the CdS-sensitized hybrid structure system as a result of the improved distribution of the CdS QDs and the effective separation of the photo-generated charges.

The superior PEC performance of the CdS-sensitized hybrid structure can be ascribed to the following reasons: as illustrated in Fig. 5, the TiO_2 nano-polyhedrons grown on TWTs not only increase the specific surface area of the electrode but also improve light utilization owing to the exposed highly active {001} facets. It is also noteworthy that a higher specific surface area can increase the interface are as between the electrode and electrolyte, which can effectively reduce the recombination rate of photo-generated electron–hole pairs and thus enhance the photocurrent density. Moreover, the TiO_2 nano-polyhedrons grown on TWTs with highly active {001} facets provide more effective area for the adsorption of CdS, thus increasing the generation of electron–hole pairs. Moreover, as the conduction band edge of CdS is higher than that of TiO_2, a type-II band structure is formed between CdS and TiO_2, facilitating the transfer of photo-generated electrons from CdS to TiO_2. The photoexcited electrons then move from CdS to TiO_2 nano-polyhedrons or move from CdS to TWTs and are gathered on the Ti substrate; this leads to a considerably reduced electron–hole recombination and enhanced photocurrent and efficiency.

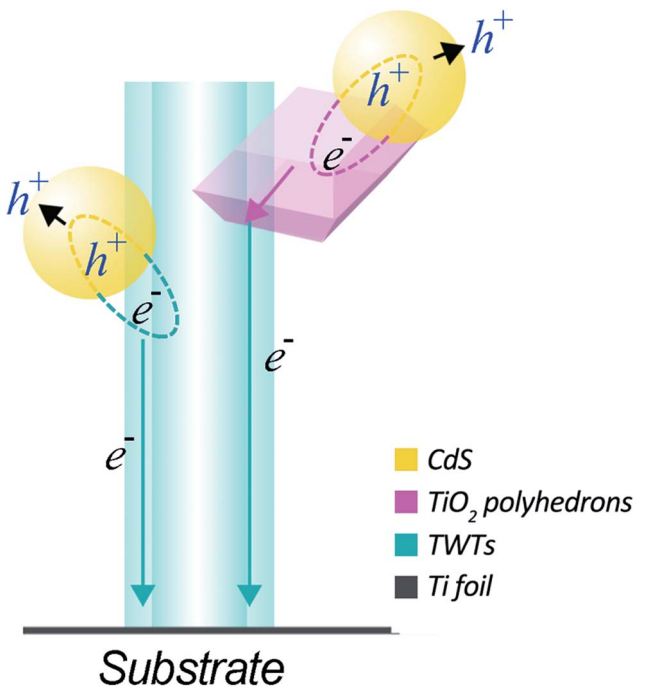

Fig. 5 Schematic showing the charge-transfer processes between CdS QDs and hybrid structure.

4. Conclusions

In summary, the TiO_2 hybrid structure with highly active {001} facets was fabricated *via* a facile method, which exhibited higher specific surface area and enhanced PEC performance. Under simulated sunlight illumination (AM 1.5 light at 100 mW cm^{-2}), J_{SC} and η of the hybrid structure were 1.36 mA cm^{-2} and 0.81%, respectively, nearly 2.4 times higher than those of TWTs. Moreover, the CdS-sensitized hybrid structure showed a superior PEC performance over the CdS-sensitized bare TWTs owing to the larger specific surface area and enhanced activity provided by nano-polyhedrons grown on the TWTs. J_{SC} and η of the CdS-sensitized hybrid structure were 2.31 mA cm^{-2} & 1.94%, respectively, about 1.5 times those of the CdS-sensitized TWTs, and the hybrid structure can boost the J_{SC} and η values of bare TWTs by up to 400%. Thus, this TiO_2 hybrid structure can be an ideal candidate to construct a photoanode for water splitting and photocatalysis.

Conflicts of interest

There are no conflicts of interest to declare.

Acknowledgements

This work was supported by the Technology Development Program of Jilin Province (Grant no. 20130206078GX).

References

1 X. Chen and S. S. Mao, Titanium Dioxide Nanomaterials: Synthesis, Properties, Modifications, and Applications, *Chem. Rev.*, 2007, **107**, 2891–2959.
2 J. Zhang, Y. Zhang, Y. Lei and C. Pan, Photocatalytic and Degradation Mechanisms of Anatase TiO_2: A HRTEM Study, *Catal. Sci. Technol.*, 2011, **1**, 273–278.
3 L. Kavan, M. Grätzel, S. E. Gilbert, C. Klemenz and H. J. Scheel, Electrochemical and photoelectrochemical investigation of single-crystal anatase, *J. Am. Chem. Soc.*, 1996, **118**, 6716–6723.
4 G. S. Li, L. Wu, F. Li, P. Xu, D. Q. Zhang and H. X. Li, Photoelectrocatalytic Degradation of Organic Pollutants Via a CdS Quantum Dots Enhanced TiO_2 Nanotube Array Electrode under Visible Light Irradiation, *Nanoscale*, 2013, **5**, 2118–2125.
5 M. Liu, J. Zheng, Q. Liu, S. Xu, M. Wu, Q. Xue, Z. Yan, H. Xiao, Z. Wei and H. Zhu, The Preparation, Load and Photocatalytic Performance of N-Doped and CdS-Coupled TiO_2, *RSC Adv.*, 2013, **3**, 9483–9489.
6 I. Mora-Seró, S. Giménez, F. Fabregat-Santiago, R. Gómez, Q. Shen, T. Toyoda and J. Bisquert, Recombination in Quantum Dot Sensitized Solar Cells, *Acc. Chem. Res.*, 2009, **42**, 1848–1857.
7 Y. Li, X. Wei, B. Zhu, *et al.*, Hierarchically branched Fe_2O_3@TiO_2 nanorod arrays for photoelectrochemical water splitting: facile synthesis and enhanced photoelectrochemical performance, *Nanoscale*, 2016, **8**, 11284–11290.
8 A. Fujishima and K. Honda, Electrochemical photolysis of water at a semiconductor electrode, *Nature*, 1972, **238**, 37.
9 M. Xu, P. Da, H. Wu, D. Zhao and G. Zheng, Controlled Sn-Doping in TiO_2 Nanowire Photoanodes with Enhanced Photoelectrochemical Conversion, *Nano Lett.*, 2012, **12**, 1503–1508.
10 P. D. Yang, D. Y. Zhao, D. I. Margolese, *et al.*, Block Copolymer Templating Syntheses of Mesoporous Metal Oxides with Large Ordering Lengths and Semicrystalline Framework, *Chem. Mater.*, 2017, **11**, 2813–2826.
11 Y. C. Wang, Y. Zhang, J. Tang, H. Y. Wu, M. Xu, Z. Peng, X. G. Gong and G. F. Zheng, Simultaneous Etching and Doping of TiO_2 Nanowire Arrays for Enhanced Photoelectrochemical Performance, *ACS Nano*, 2013, **7**, 9375–9383.
12 N. K. Allam, F. Alamgir and M. A. El-Sayed, Enhanced Photoassisted Water Electrolysis Using Vertically Oriented Anodically Fabricated Ti-Nb-Zr-O Mixed Oxide Nanotube Arrays, *ACS Nano*, 2010, **4**, 5819–5826.
13 B. Sun, *et al.*, Decoration of TiO_2 Nanotube Arrays By Graphitic-C_3N_4 Quantum Dots with Improved Photoelectrocatalytic Performance, *Appl. Surf. Sci.*, 2017, **394**, 479–487.
14 K. Naito, T. Tachikawa, M. Fujitsuka and T. Majima, Single-molecule observation of photocatalytic reaction in TiO_2 nanotube: importance of molecular transport through porous structures, *J. Am. Chem. Soc.*, 2009, **131**, 934–936.
15 J. H. Ping, *et al.*, High-Performance Large-Scale Flexible Dye-Sensitized Solar Cells Based on Anodic TiO_2 Nanotube Arrays, *ACS Appl. Mater. Interfaces*, 2013, **20**, 10098–10104.
16 G. Liu, X. Liu, L. Wang, *et al.*, Hierarchical $Li_4Ti_5O_{12}$-TiO_2, microspheres assembled from nanoflakes with exposed $Li_4Ti_5O_{12}$-TiO_2, (011) and anatase TiO2, (001) facets for high-performance lithium-ion batteries, *Electrochim. Acta*, 2016, **222**, 1103–1111.
17 Y. Tang, P. Wee, Y. Lai, *et al.*, Hierarchical TiO_2 Nanoflakes and Nanoparticles Hybrid Structure for Improved Photocatalytic Activity, *J. Phys. Chem. C*, 2015, **116**, 2772–2780.
18 F. Zhu, H. Dong, Y. Wang, D. P. Wu, J. M. Li, J. L. Pan, Q. Li, X. C. Ai, J. P. Zhang and D. S. Xu, Dual-functional hetero-structured TiO_2 nanotrees composed of rutile trunks and anatase branches for improved performance of quantum dot-sensitized solar cells, *Phys. Chem. Chem. Phys.*, 2013, **15**, 17798–17803.
19 M. Lazzeri, A. Vittadini and A. Selloni, Structure and Energetics of Stoichiometric TiO_2 Anatase Surfaces, *Phys. Rev. B*, 2002, **65**, 119901.
20 J. G. Yu, J. X. Low, W. Xiao, P. Zhou and M. Jaroniec, Enhanced Photocatalytic CO_2-Reduction Activity of Anatase TiO_2 by Coexposed {001} and {101} Facets, *J. Am. Chem. Soc.*, 2014, **136**, 8839–8842.
21 X. Han, Q. Kuang, M. Jin, Z. Xie and L. Zheng, Synthesis of titania nanosheets with a high percentage of exposed (001)

facets and related photocatalytic properties, *J. Am. Chem. Soc.*, 2009, **131**, 3152–3153.

22 A. Selloni, Crystal growth: anatase shows its reactive side, *Nat. Mater.*, 2008, **7**, 613–615.

23 C. Chen, R. Hu, K. G. Mai, Z. M. Ren, H. Wang, G. D. Qian and Z. Y. Wang, Shape Evolution of Highly Crystalline Anatase TiO_2 Nanobipyramids, *Cryst. Growth Des.*, 2011, **11**, 5221–5226.

24 G. Liu, H. G. Yang, X. Wang, L. Cheng, J. Pan, G. Q. Lu and H. M. Cheng, Visible light responsive nitrogen doped anatase TiO_2 sheets with dominant {001} facets derived from TiN, *J. Am. Chem. Soc.*, 2009, **131**, 12868–12869.

25 H. G. Yang, C. H. Sun, S. Z. Qiao, J. Zou, G. Liu, S. C. Smith, H. M. Chen and G. Q. Lu, Anatase TiO_2 Single Crystals with a Large Percentage of Reactive Facets, *Nature*, 2008, **453**, 638–641.

26 H. G. Yang, G. Liu, S. Z. Qiao, C. H. Sun, Y. G. Jin, S. C. Smith, J. Zou, H. M. Chen and G. Q. Lu, Solvothermal Synthesis and Photoreactivity of Anatase TiO_2 Nanosheets with Dominant {001} Facets, *J. Am. Chem. Soc.*, 2009, **131**, 4078–4083.

27 Y. P. Zhang, C. Z. Li and C. X. Pan, N + Ni Codoped Anatase TiO_2 Nanocrystals with Exposed {001} Facets Through Two-Step Hydrothermal Route, *J. Am. Ceram. Soc.*, 2012, **95**, 2951–2956.

28 S. U. M. Khan, M. Al-Shahry and W. B. Ingler Jr, Efficient Photochemical Water Splitting by a Chemically Modified n-TiO_2, *Science*, 2002, **297**, 2243–2245.

29 W. J. Sheng, B. Sun, T. L. Shi, X. H. Tan, Z. C. Peng and G. L. Liao, Quantum Dot-Sensitized Hierarchical Micro/Nanowire Architecture for Photoelectrochemical Water Splitting, *ACS Nano*, 2014, **8**, 7163–7169.